LA-UR-17-28572
Approved for public release; distribution is unlimited.

Title: June 2017 Ancho Canyon RF Collects: Final Report

Author(s): Junor, William
Layne, John Preston
Goglio, Joshua Henry
Quintana, Bobby Arthur
Snelson-Gerlicher, Catherine Mary
Goorley, John Timothy

Intended for: Report

Issued: 2017-09-21

June 2017 Ancho Canyon RF Collects: Final Report

FINAL

Bill Junor, John Layne, Josh Goglio,
Bobby Quintana, Cathy Snelson-Gerlicher,
Tim Goorley

Los Alamos National Laboratory September 18, 2017

Contents

List of Figures

List of Tables

Chapter 1

Executive Summary

We report the results from the June 8, 2017, Ancho Canyon RF collection. While bright, electromagnetic signals were seen close to the firing point, there were no detections of signals from the explosively-fired fuse (EFF) at a collection point about 600 m distant on the East Mesa. The East Mesa site was unable to collect data because the uninterruptible power supply (UPS) was exhausted by the time of the shot.

We did see signals from the EFF at the Bunker 57 antennas, about 123 m distant from the Point 88 firing point. The strength of these signals is consistent with our limited knowledge of the collection antenna performance and the use of the standard model to predict the electric field strength.

From our knowledge of the geometry of the EFF loop and the current in the loop in this test, and from measurements at the Bunker 57 site, we predict that we would have seen signals of about 50 mV at 3.67 MHz in a 100 kHz channel on the Rohde & Schwarz HE010 antennas at the East Mesa location. The noise floor there is about 0.113 mV (based on the March 2017 collects). Thus we would have had an SNR of ≈53 dB from the collect, had the data collection system been running.

Chapter 2

Introduction

The feasibility of using electromagnetic (EM) and seismo-acoustic (SA) signals collaboratively to monitor nuclear weapon testing is being investigated. The facilities at Ancho Canyon offer the opportunity to simulate — at a crude level — the EM and SA signatures. The seismo-acoustic signal can be initiated by a chemical explosion.

The electromagnetic signal may be emulated by the use of an explosively-fired fuse (EFF). These devices can generate a narrow pulse, approximately 1 μs wide, by abruptly interrupting the flow of a very large current.

The EM signature of this event is known poorly, though anecdotal information suggests that it should be readily observed at low radio frequencies.

A test shot with an EFF in a standard configuration was conducted on March 2, 2017. While EM energy was generated in the shot, no far-field signal was detected. We proposed that the likely field strength from the shot was insufficient to be seen against the strong ambient noise background. We developed a new EFF configuration with a large loop to improve the strength of the radiated signal.

We conducted an EFF test shot on June 8, 2017, with the larger loop as part of the EFF circuitry. Our goal was to improve the radiated electromagnetic signal from the event such that it could be detected at the East Mesa location.

2.1 Prior work

We had conducted a trial radio frequency collection against the firing of an EFF on March 5, 2017 (Junor *et al.*, 2017). Our goals for that test collect were:

- to exercise the RF collection system,
- to develop a RF collection plan for future experiments,
- to coordinate the activities at the firing site in Ancho Canyon with the RF data collection,
- to assess the size of the electromagnetic signal from the EFF, and
- to assess the electromagnetic background against which the EFF-generated EM signals must be detected.

As a goal of future joint collects between the seismo-acoustic sensors and the radio frequency sensors is improved geolocation of events, there is a loose requirement that the SA and EM sensors be roughly co-located. The SA sensors are either in the permanent network around Los Alamos, or as part of a temporary network installed nearby on the mesas.

In the March 2017 collect, we chose two sites for our RF measurements: one on the East Mesa overlooking the firing point at Point 88 in Ancho Canyon, and the other at the firing point itself. The East Mesa site had a direct line-of-sight to the firing point. The RF sensors at the firing point were an "insurance" measure to make sure we saw some RF signals associated with the event, should the signals at the East Mesa be too weak for detection.

The firing point sensors saw a large signal from the event. However, the signal was so large that it saturated all collection channels. The recorded voltage from the energized loop was at least 0.2 V. Since the antenna used for this collection was a cheap Centerfire discone with an Antenna Factor of 20 dB(1/m) or larger, this means that the *near-field* electric field strength was at least 2 V/m.

The East Mesa collection system saw no EFF-caused signal above the noise floor of a few mV in the March 2 test. The East Mesa location is at about 600 m from the firing point and so should be in the far-field for the EFF source for frequencies above ≈ 5 MHz.

Chapter 3

Development of new EFF loop

In the post-event analysis of the March 2 shot, we concluded that the noise floor on the East Mesa had been significantly larger than anticipated and that this had contributed to the non-detection of any EFF-caused signal.

Small loops are notoriously inefficient radiators of electromagnetic energy. So, while the loop used in March was energized by a very large instantaneous current, very little of this energy was converted into far-field electromagnetic signals.

For a small loop, the azimuthal, far-field, electric field, E_ϕ, is

$$E_\phi \;=\; \frac{120\pi^2[I]\sin\theta A}{r\lambda^2} \tag{3.1}$$

where $[I]$ is the retarded current, A is the area of the current loop, λ is the wavelength and r is the distance from the loop (Kraus & Marhefka , 2002; Balanis , 2005). The loop is small so we can assume that the current is the same everywhere in the loop. Since the electric field is proportional to the cross-sectional area of the loop, we decided to attach a large loop to the EFF circuit.

The standard EFF loop is 2.6 cm × 35.5 cm. We augmented this loop ("6.5″ switch") with a loop 44 cm on a side thus giving a factor of 20.98 in area. The larger loop introduces additional inductance and this would increase the time constant of the EFF circuit ($\tau = L/R$ where L is the inductance in Henrys and R is the resistance in Ohms). Using the formulae in Rosa & Grover (1912), we estimated the new loop inductance as 92.3 μH. (We adopted dimensions of 44.0 cm × 44.0 cm, with a strip width of 1.5 m, and strip thickness of 0.4318 mm for these calculations.)

To keep the total inductance in the capacitor bank/EFF/loop circuit similar to that of the first experiment (and thus keep the time constant similar), we chose to run 4 capacitor banks in parallel, rather than using just one bank as in the March 2 experiment. This has the consequence that we do not charge the banks to the same voltage as before but only to half the peak voltage *i.e.* 5 kV. This results in twice the amount of charge as in the first experiment and therefore twice the current, all other factors being equal. The total energy in the system is the same in both experiments.

The resulting inductance budget is given in Table 3.1 and is compared to the budget for the first experiment. The total inductances for the two experiments are similar and

therefore the L/R time constants will be similar. (The resistance, R, is dominated by the EFF which is the same in the March and June experimental configurations.)

Component	March 2	June 8
Switch header	21	0
6.5″ switch	58	54
Capacitor bank	42	10.5
Shot cables	92	19.3
Antenna loop	0	92.3
Total	213	176.1

Table 3.1: Inductance budgets for the March 2 and June 8 experiments. All values in nH.

Figure 3.1 shows the larger EFF loop at the firing point. The blue cables of the right of the loop are coaxial cables coming from the capacitor bank header in the bunker. The grey and yellow structure around the light blue cables (inner of coaxial cables) is a Faraday rotation sensor. The EFF itself (without explosive charge) can be seen (just) on the left-most part of the wooden table. The silver-colored aluminum foil is connected to the single ground point out of picture.

Figures 3.2 and 3.3 show the large loop and the EFF in more detail.

Figure 3.1: EFF and large radiative loop at Point 88.

Figure 3.2: Large radiative loop at Point 88 (44 cm on a side), looking along the axis of the loop.

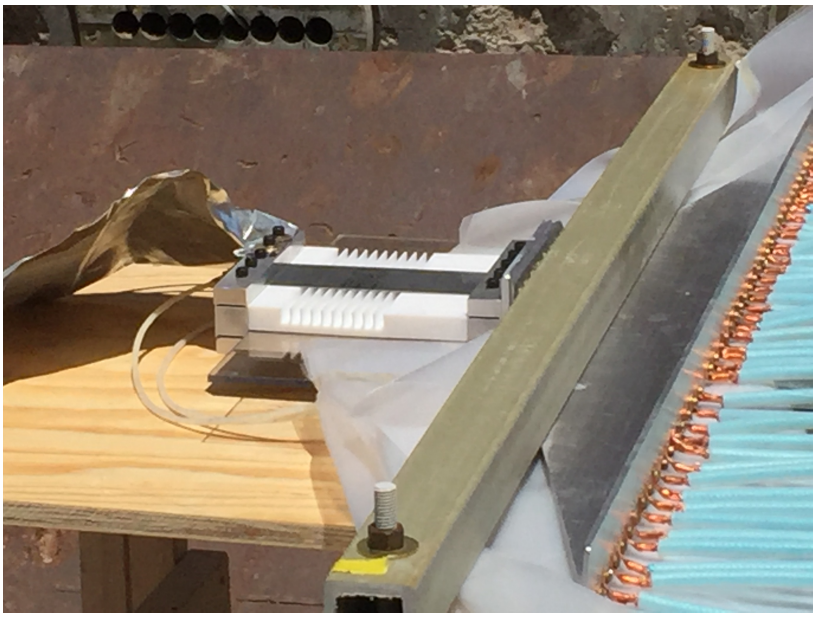

Figure 3.3: EFF (white corrugated former with Invar strip on top at center, with cable attachment assembly to the right.

Chapter 4

Technical approach

The current pulse width is estimated to be $\approx 1\,\mu$s. Thus, the anticipated spectrum is expected to be centered around 1 MHz. Of course, the rise and fall times of the pulse are much faster so there should be additional electromagnetic information available at higher frequencies.

The anticipated polarization of the radiated electric field in the azimuthal plane is vertical. This would be expected from a consideration of the current flow in the circuit (Balanis , 2005).

We have available a number of Rohde & Schwarz HE010 active monpole antennas (Rohde & Schwarz , 2017a) which have a frequency coverage from 20 kHz to ≈80 MHz. These are mounted vertically and so they are sensitive to vertical polarization only. Cheng Ho made available a 3-axis (x,y,z) custom variant of this antenna to give us a horizontally polarized sensor.

We also used a pair of cheap Centerfire discone antennas at the Point 88 firing point itself and a second pair close to Bunker 57. Bunker 57 is intermediate in distance between Point 88 and the East Mesa location. The Point 88 antennas were intended to measure the near-field electric field strength while the Bunker 57 system was an insurance measure.

4.1 East Mesa collection site

We set up a data acquisition system on the East Mesa overlooking the Point 88 firing point. This location is in the far-field of most of the anticipated radiated signal. The distance from the center of the antenna array to the firing point at Point 88 is 595 m.

To allow for geolocation, we distributed 6 HE010 antennas along the mesa edge over about 350 feet in extent. The placement was not ideal since this had a roughly linear pattern but we tried to find as much spatial diversity as the terrain would allow.

The 3-axis antenna was located above the trailer hosting the data acquisition system.

On the East Mesa, we captured the signals on a National Instruments PXIe-1082 crate using two kinds of data aquisition cards — NI 5122 and NI 5154. The NI 5122 cards have 2 channels per card and a 100 MHz sample rate. The NI 5154 cards have 2 channels per card and a 1 GHz sample rate. The systems were disciplined with a NI GPS card (NI PXI 6682-H). We used a 10 ms window on the NI 5122 card and a 1 ms window on the

NI 5154 card. Each window was centered on the top of the GPS minute *i.e.* we used a 50% pre-trigger.

To avoid saturation of the active circuitry and, potentially, the data acquisition systems, by strong FM broadcast stations and to avoid aliasing from the same, we inserted Mini-Circuits low pass filters in each HE010 channel. These BLP-50+ filters suppress signals above 48 MHz (MiniCircuits , 2017).

Because we have a remote location and a direct firing control system trigger is impractical there, we required that the EFF event and data collection at all RF collection sites would happen at the top of the GPS minute. Moreover, we are required to vacate the East Mesa location during the EFF event and thus the East Mesa data acquisition system has to run autonomously. Thus, collecting at the top of each minute, when the exact firetime minute is not known ahead of time, is a good solution. In addition, the collections for the "empty" tops-of-minute allows us to characterize the RF background.

The East Mesa data acquisition systems were powered from one of two APC UPS systems. Each of these systems would allow the data acquisition to run for about 4 hours continuously. Using UPS systems allows us to avoid impulsive ignition noise from gasoline-powered generators. (However, UPS systems do have inverters to change the power from ≈ 12 VDC to 110 VAC. Potentially, these could be a source of noise.)

The time-of-flight from the firing point to the East Mesa antennas is about 2 μs.

Figure 4.1 show the view up the canyon towards the Point 88 bunker from the East Mesa collection location. In the foreground, we have a Rohde & Schwarz active monopole mounted on a tripod.

4.2 Bunker 57 collection system

At the Bunker 57 location, we deployed two Centerfire discones. We split the signal from each of these into two channels of a 4 channel Tektronix DPO7254C digital oscilloscope. The voltage settings on each channel were bracketed to allow capture of the unknown (in voltage) signal from the firing of the capacitor bank with the larger loop. The data acquisition was triggered by an external GPS receiver at the top of the GPS minute.

We tested the liveness of the Bunker 57 data acquisition system with a FIST portable pulser unit (Ho, Frigo & Haynes , 2014). The FIST unit generates 3 short pulses within 1 μs. The broadband signal peaks at a few 10s of MHz. The pattern of 3 short pulses allows us to discriminate between the pulser output and random noise pulses from lightning, power lines, or other source. We also tested the system by firing a bridgewire at the Point 88 firing point using the same control and triggering system as for the main test.

The Bunker 57 antennas are 114 m from the EFF at Point 88 and lie at azimuths of 25° (L) and 22° (R) with respect to the EFF loop axis. (Left (L) and right (R) are with respect to the direction facing the Point 88 firing point from behind the Bunker 57 antennas.

4.3 Point 88 collection system

We connected 2 discone antennas to the Point 88 bunker data acquisition system. We fanned out the signal from each antenna 4 ways so that we might bracket the range of

Figure 4.1: View from East Mesa collection location towards Point 88 firing point. The firing point itself is partially obscured by trees in this picture.

the data acquisition system and avoid saturation. Each channel of the 300 MHz data acquisition rack has a 12-bit depth. The 1 GHz data acquisition system has only an 8-bit depth. Since we did not anticipate much signal above 100 MHz, we opted for the use of the 12-bit system.

The axis of the large firing point loop was oriented at 20° East of North. The nulls of the far-field radiation pattern are along the loop axis. (At least, this is true for a small loop in free space. The radiation pattern for this loop is likely to be distorted significantly due to the proximity of the ground and nearby scattering structures.) The main axis of the radiation pattern was thus aimed down the canyon towards the East Mesa location *i.e.* in azimuth 110° E of N.

A near-field antenna was located in this azimuth, separated by 18.84 m from the nominal firing point (taken to be the end of the EFF which was connected to the single ground). A second near-field antenna was located along the loop axis on the concrete apron to the west (*i.e.* in azimuth 200° E of N. This antenna was separated by 23.45 m from the nominal firing point. The firing point antennas were located on supports up about 3 m. (Separation distances given here are from the nominal firing point to the feed point of the antenna.)

4.3.1 Centerfire discone performance

We used several Centerfire Deluxe Discone antennas (Centerfire , 2017). These are cheap and have nominal frequency coverage of 30–1300 MHz.

Discones are generally used for their wide frequency coverage; however, they have poor gain at any frequency (typically around 0 dBi). The frequency coverage of these antennas is not ideal for our application where we expect much of the energy to be at about a few MHz. However, antennas designed specifically for such frequencies would be quite large and would require mounting on large support structures. (In general, the physical size of an antenna scales with the wavelength. Exceptions to this are compact antennas such as short monopoles and discones which have very compromised performances. Some mitigation of the limited performance is possible with matching networks and pre-amplification.) Since we are using the Centerfire discones close to the source, we felt that they were a reasonable compromise in terms of cost/performance. Moreover, antennas this close to the firing point are exposed to flying debris.

Because the Centerfire discones are cheap, they also do not have any published performance specifications. Measuring their performance on a test range requires a modicum of care and some reasonable test equipment.

4.3.2 Antenna Factor

The Antenna Factor, AF, relates the ability of an antenna to convert the sampled electric field illuminating the antenna into a voltage at the antenna terminals *i.e.*

$$AF = \frac{E}{V} \tag{4.1}$$

or in logarithmic form

$$AF[\mathrm{dB\,1/m}] = E[\mathrm{dB\,V/m}] - V[\mathrm{dB\,V}] \tag{4.2}$$

The Antenna Factor for a 50 Ohm antenna system is related to its gain by

$$AF = \frac{9.73}{\lambda\sqrt{G}} \tag{4.3}$$

where λ is the wavelength in m, and G is the gain. However, for Equation 4.3 to hold, we require that

- the radiation field and the antenna polarization be matched,
- the antenna is excited by a plane wave *i.e.* the antenna is in the far field, and
- the antenna is impedance matched.

We have looked at similar discone antennas with published specifications. These are:

- AIR 802 Ultra Wideband discone Antenna, 100–1000 MHz, 1–3.5 dBi Gain (AIR 802 , 2017),
- Antenna Research Associates CMA-750, 70–500 MHz, -0.8–1.1 dBi (Antenna Research Associates , 2017),
- Diamond Antenna D130NJ Super Discone Antenna, 25–1300 MHz, 2 dBi nominal (Diamond Antenna , 2017),
- Hascall-Denke DC113X4, 113–420 MHz DC113X4, 0–2.5 dBi (Hascall-Denke , 2017)

Assuming that the Centerfire antenna gain is a nominal 0 dB and that its impedance is 50 Ohms throughout its range, we can plot its nominal Antenna Factor as a function of frequency (Figure 4.2). This is compared to the Antenna Factor performance for the ARA-750 discone in Figure 4.3.

However, we are really interested in the performance of the Centerfire antenna well below 50 MHz. In this frequency regime, the antenna is poorly matched in impedance. This will cause the Antenna Factor to rise steeply at these low frequencies.

We do not have good facilities to measure the performance of antennas at low frequencies. However, we have tried to estimate the performance of the Centerfire discone by a direct comparison with a calibrated antenna, an Aaronia BiCoLog 20100e (Aaronia , 2017). The Aaronia Antenna Factor curve is plotted in Figure 4.4. The performance of this antenna has been measured down to ≈20 MHz only.

We illuminated the Centerfire discone and the Aaronia 20100e antenna at discrete frequencies in the range 15–100 MHz and measured the output of the antennas on a spectrum analyzer. We controlled for the placement of the antennas and the polarization. The difference in outputs from the antennas is shown in Figure 4.5.

Since the Antenna Factor of the 20100e BiCoLog antenna is known, we can estimate the Antenna Factor of the discone. Using Equation 4.3, we can write

$$\frac{\mathrm{AF}_{\mathrm{discone}}}{\mathrm{AF}_{\mathrm{bicolog}}} = \sqrt{\frac{G_{\mathrm{bicolog}}}{G_{\mathrm{discone}}}} \tag{4.4}$$

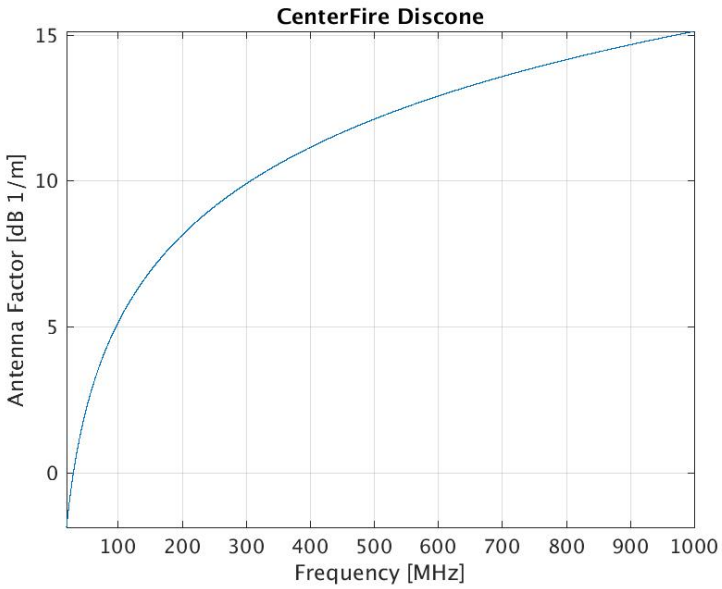

Figure 4.2: Antenna Factor for Centerfire discone antenna with nominal performance.

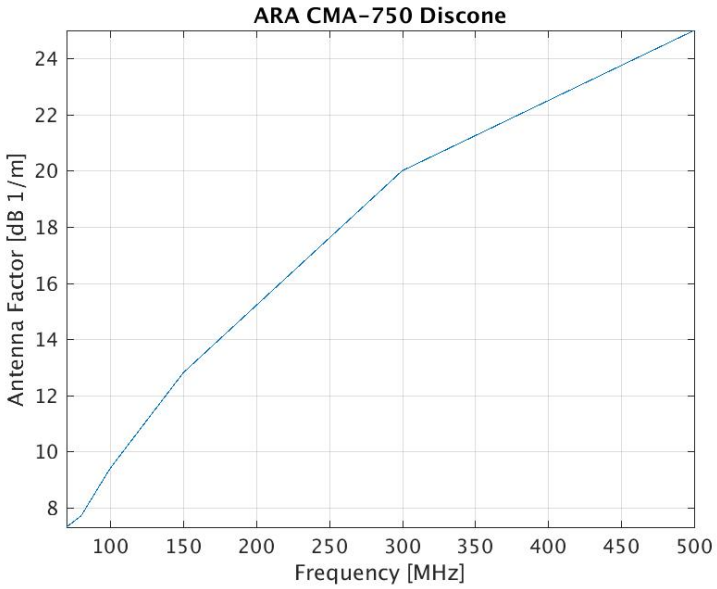

Figure 4.3: Antenna Factor as a function of frequency for ARA CMA-750 discone antenna.

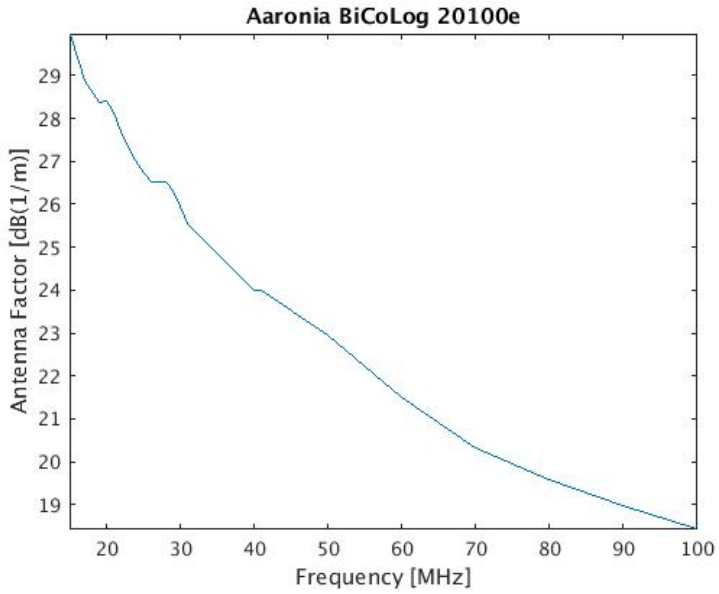

Figure 4.4: Antenna Factor as a function of frequency for Aaronia 20100e BiCoLog antenna.

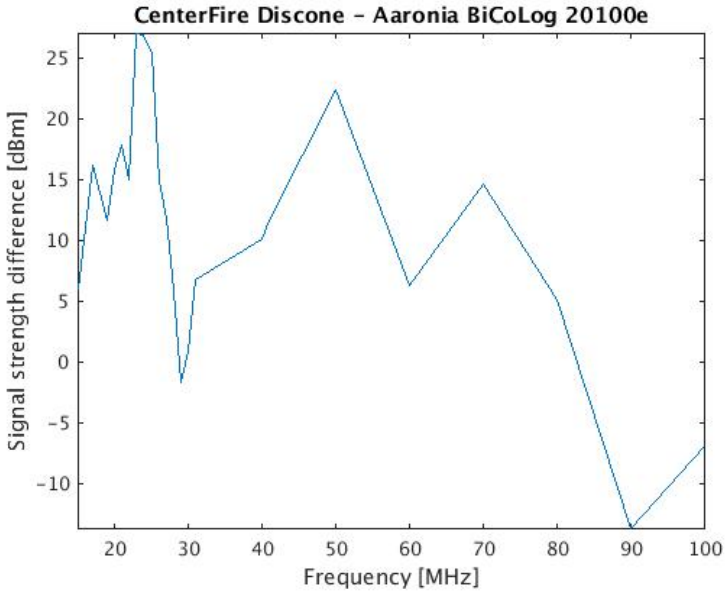

Figure 4.5: Difference in power measured by Centerfire discone and Aaronia 20100e BiCoLog antenna.

and so

$$\mathrm{AF}_{discone}\left[\mathrm{dBm}^{-1}\right] = \mathrm{AF}_{bicolog}\left[\mathrm{dBm}^{-1}\right] + \frac{1}{2}\left(G_{\mathrm{bicolog}} - G_{\mathrm{discone}}\right)[\mathrm{dB}] \quad (4.5)$$

and since power is directly proportional to antenna gain, we can replace the difference in gains between the antennas with the difference in power received by those antennas *i.e.*

$$\mathrm{AF}_{discone}\left[\mathrm{dBm}^{-1}\right] = \mathrm{AF}_{bicolog}\left[\mathrm{dBm}^{-1}\right] + \frac{1}{2}\left(P_{\mathrm{bicolog}} - P_{\mathrm{discone}}\right)[\mathrm{dB}] \quad (4.6)$$

The average power difference for frequencies 20 MHz and below is 12.37 dB while the average Antenna Factor for the BiCoLog in this range is 28.91 dBm^{-1}. Thus, our estimate for the Centerfire discone Antenna Factor in this frequency regime is $\approx 23\,\mathrm{dBm}^{-1}$.

Of course, this is a very crude estimate but it gives us a sense of the antenna's performance. To do this correctly, we would require a large test range and good control over reflections.

Alternatively, we could model the discone antenna's performance in NEC (Numerical Electromagnetics Code (Burke & Poggio , 1981a,b,c; Burke , 1992). We have not done this yet.

We will adopt a value of $23\,\mathrm{dBm}^{-1}$ for the Antenna Factor of the Centerfire discones as a working value.

4.4 Far-field and near-field

The far-field region is where electromagnetic radiation propagates away from the source, without any back-interaction. The fields in this region are dipole-like. The far-field electromagnetic radiation field strengths fall off as 1/r. By contrast, the near-field region is governed by multipole fields which do not radiate. In this region, the phase relationship between the E and B fields is complex. See, for example, OSHA (1990)).

The transition between near-field and far-field is vaguely defined. For electromagnetically short radiators — such as we have at the EFF — the near-field is the region within a wavelength *i.e.* $r << \lambda$.

Since one component of the electromagnetic signature is expected at $\approx$ 1 MHz, the near-field region will be inside ≈300 m. The far-field region is typically defined to be $r >> 2\lambda$. Thus, the discones at the firing point are well within the near-field for some of the electromagnetic signal, while the East Mesa location is just at the inner edge of the far-field for most of the radiation.

4.5 Data acquisition system at Ancho Canyon

We used 2 Centerfire "Deluxe Discone" antennas (Centerfire , 2017) close to the shot table. Our concern was that the close-in antennas could be damaged by flying debris from the explosion. These antennas are more than adequate for the likely field strengths close to the shot table.

Coaxial cables were run from all of the antennas directly to the bunker patch panel. The phase centers of the antennas are unknown. Potentially, this could introduce errors

of $\approx 0.5\,\mathrm{m}$ in geolocation but this is a minor factor when compared to other errors in the analysis. The antennas were mounted on masts and the antenna bases were about $3\,\mathrm{m}$ above the ground. The positions of the antennas and the position of the firing table on which the EFF was placed were measured using a Topcon GRS-1 GPS receiver (Topcon , 2017).

4.6 Firing point and collection locations

In the following figures (Figures 4.6, 4.7, 4.8), we show the locations of the Point 88 firing point, the discones near the firing point, the Bunker 57 antennas ("L antenna"), and the East Mesa antennas ("Antenna #4").

Figure 4.6: Large-scale view encompassing the collection sites and the Point 88 firing point in Ancho Canyon. (Taken from Google Earth.)

Figure 4.7: Zoomed-in view encompassing the collection sites and the Point 88 firing point in Ancho Canyon. (Taken from Google Earth.)

Figure 4.8: View encompassing the Bunker 57 collection site and the Point 88 firing point in Ancho Canyon. (Taken from Google Earth.)

Chapter 5

Analysis

5.1 Timing chain

In Figure 5.1, we show the timing of events in the arming and firing chain.

5.2 Data collection at Bunker 57

5.2.1 Testing

We conducted liveness tests of the Bunker 57 data acquisition system using the FIST portable pulser. Figure 5.2 shows a representative collect.

We also fired a bridgewire at the Point 88 firing point using the same timing and controls as used for the EFF shot. This is a much weaker signal but we did detect this on the two most sensitive channels at the Bunker 57 location (Figure 5.3).

5.2.2 EFF shot

The signal from the EFF shot was detected on the two most sensitive channels. These were Channels 3 and 4 which were tied to the left-most discone antenna (designated as 'L'). These signals are shown in Figures 5.4 and 5.5.

Our intention had been to run the portable pulser in parallel with the EFF shot to create a fiducial signal in the collected record. However, because the EFF shot was delayed the portable pulser ran out of power before the actual shot. Hence, no fiducial signal was available.

The spectrogram of the event (Figure 5.6) shows that the discharge of the capacitor banks (at $\approx 20\,\mu$s) radiates signals below 15 MHz with a peak near 3.67 MHz. The radiation from the EFF happens at about $67\,\mu$s and contains signals up to ≈ 35 MHz.

The peak voltage seen on the most sensitive channel (Channel 4) is 11.2 mV (after high-pass-filtering). Assuming a nominal Antenna Factor of $23\,\mathrm{dBm}^{-1}$ and allowing for attenuation of the signal in the cable between the antenna and the oscilloscope (3.2 dB) and factoring in the 3 dB in the splitter between channels 3 and 4, we estimate that the electric field strength at the B antenna at the Point 57 bunker in this direction is $\approx -9.8\,\mathrm{dB\,V/m}$ or $\approx 0.324\,\mathrm{V/m}$ at 122.9 m from the Point 88 firing point.

We can estimate the field strength at the Bunker 57 L antenna using Equation 3.1. The principal axis of the EFF and loop is at 20° E of N. The Bunker 57 L antenna lies at 45° E of N relative to the firing point. Thus the L antenna lies close to the null of the EFF loop. We will use $\theta = 25°$. We are assuming that the radiation is in the far-field and that the azimuthal dependence and polarization is close to that of a small loop in free space.

The temporal profile of the current in the loop during the shot is shown in Figure 5.7. The peak current in the loop is 520 kA.

To get the predicted electric field strength at the Bunker 57 L antenna, first we have spectrally decomposed the current profile to give a current power spectral density profile (Figure 5.8). Using Equation 3.1, we then calculated the electric field strength as a function of frequency at Bunker 57 (Figure 5.9). The predicted electric field strength is 0.596 V/m.

From the spectral decomposition of the collected data, the measured voltage at the peak at 3.67 MHz is 0.854 mV. Using Equation 4.2, we estimate the Centerfire discone Antenna Factor to be 28.4 dBm^{-1}. This should be compared with the crude laboratory measurement where we found the Antenna Factor to be about 23 dBm^{-1} at $\approx$ 20 MHz.

Given the crudity of our field measurements and our antenna measurements, and our assumptions about the propagation from the firing point to the collection system, this seems like fairly good agreement. As we go down in frequency, the Antenna Factor will increase from its estimated value at 20 MHz.

As a final check of our assumptions, we have estimated the electric field strength as a function of frequency at Bunker 57 collection point using the spectral decomposition of the measured voltage signal. We have adopted 23 dB(1/m) for the Centerfire discone Antenna Factor. Figure 5.10 shows the estimated electric field; the average value of the electric field is 8.22 dB(V/m). This plot should be compared with Figure 5.9 which shows the predicted electric field based on the capacitor bank current profile.

The agreement between Figures 5.9 and 5.10 seems reasonable, given that we have adopted a single (frequency-independent) number for the Antenna Factor, and we have high-pass filtered (cut-off 1.5 MHz) the Bunker 57 data. We know also that the spectral power from the EFF signal is concentrated below $\approx$5 MHz (Figure 5.6) because of filter effects that are not included in our simple model.

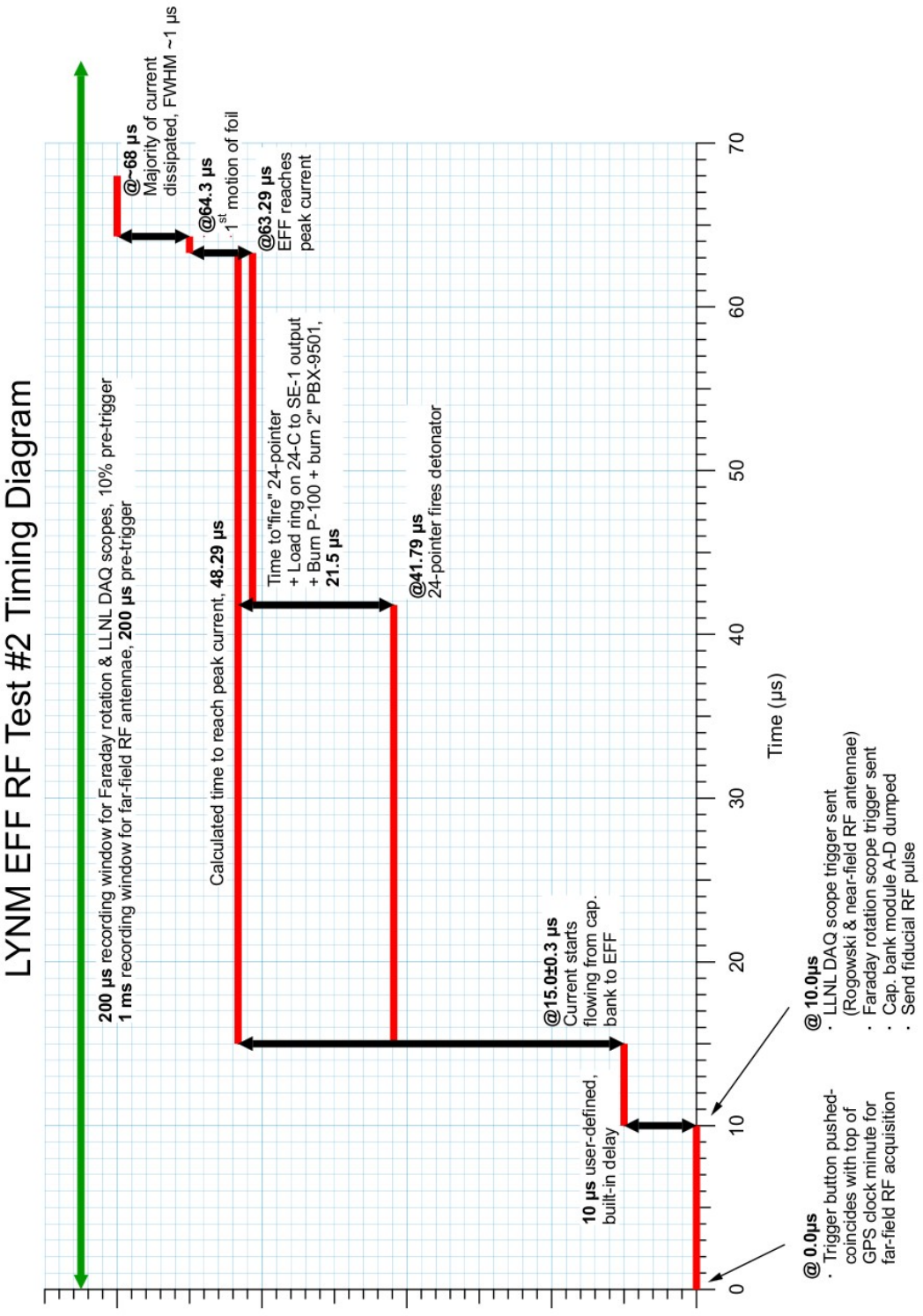

Figure 5.1: Timing diagram for the June 8, 2017, EFF shot at Ancho Canyon. (Figure from Erik Haroz.)

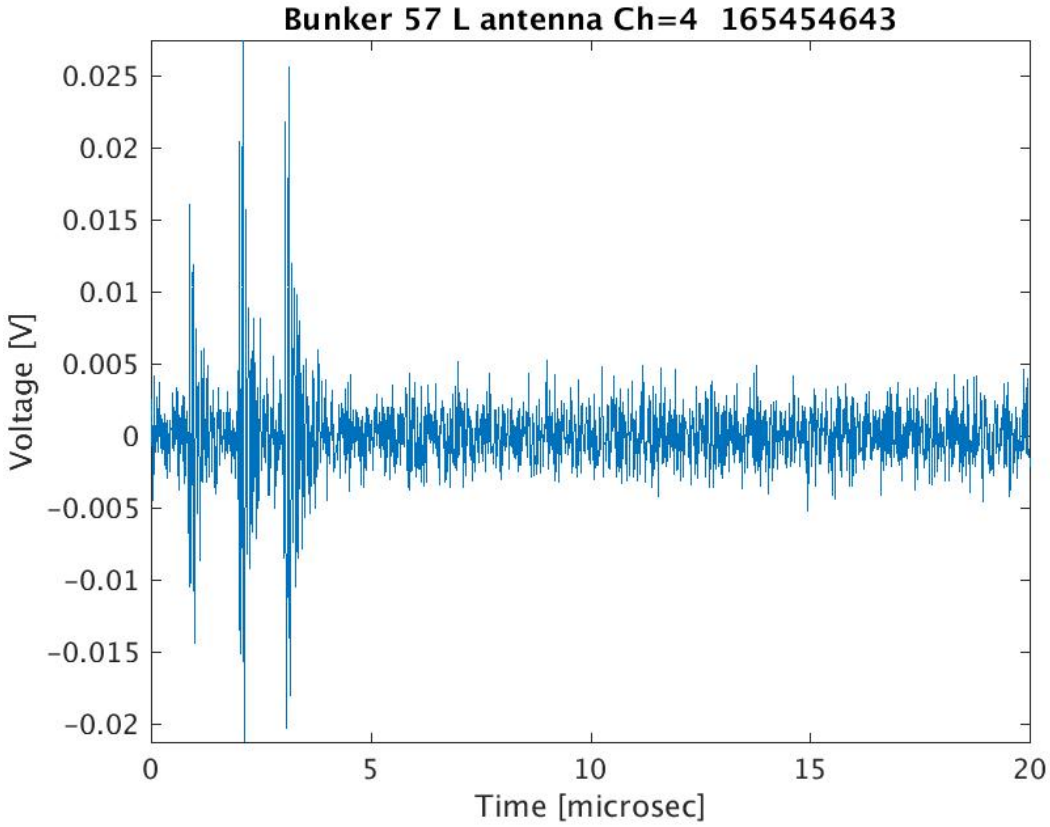

Figure 5.2: Pulser check for Bunker 57 data acquisition system. The portable pulser emits 3 narrow pulses within 3 μs just after the top of the GPS minute. These signals were seen on all 4 channels of the Bunker 57 data collection system. The filename labeling uses the data acquisition system's internal clock. This is several seconds behind the actual GPS time.

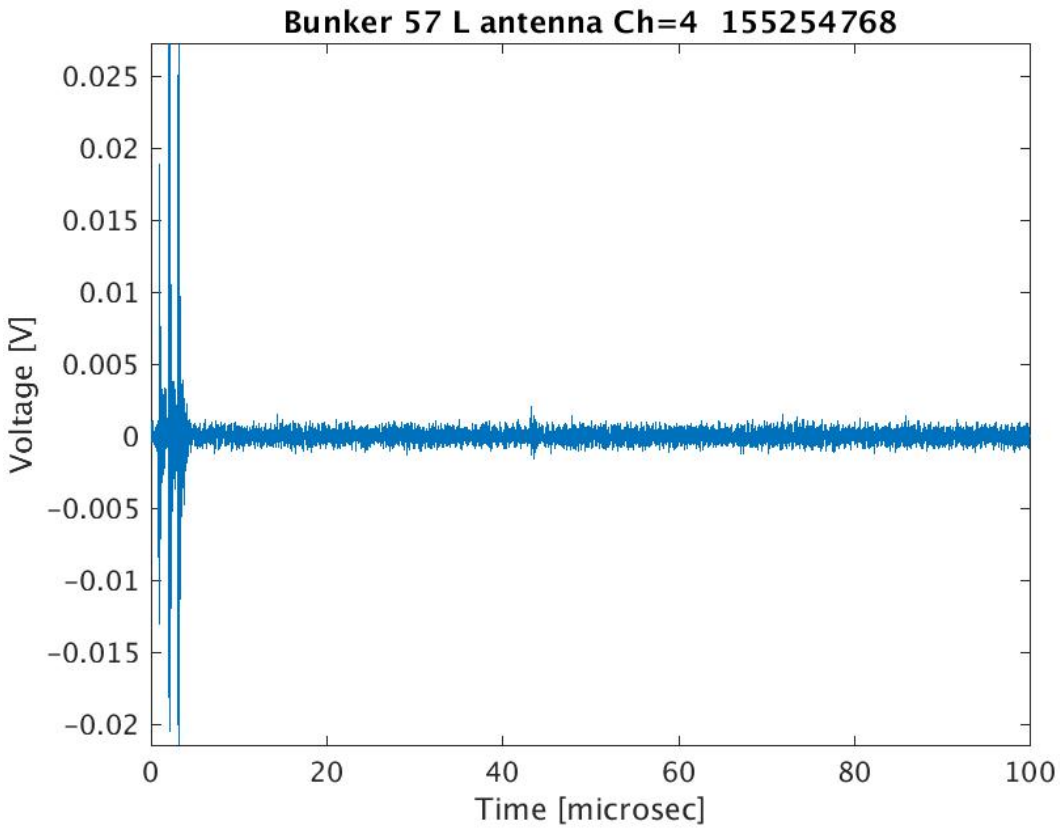

Figure 5.3: Bridgewire test for Bunker 57 data acquisition system. The signal from the triggering of the bridge wire is seen at about 42 μs after the top of the GPS minute (0 in this plot). The portable pulser signals can also be seen just after the top of the GPS minute. This signal was seen on one other channel of the Bunker 57 data collection system. The filename labeling uses the data acquisition system's internal clock. This is several seconds behind the actual GPS time.

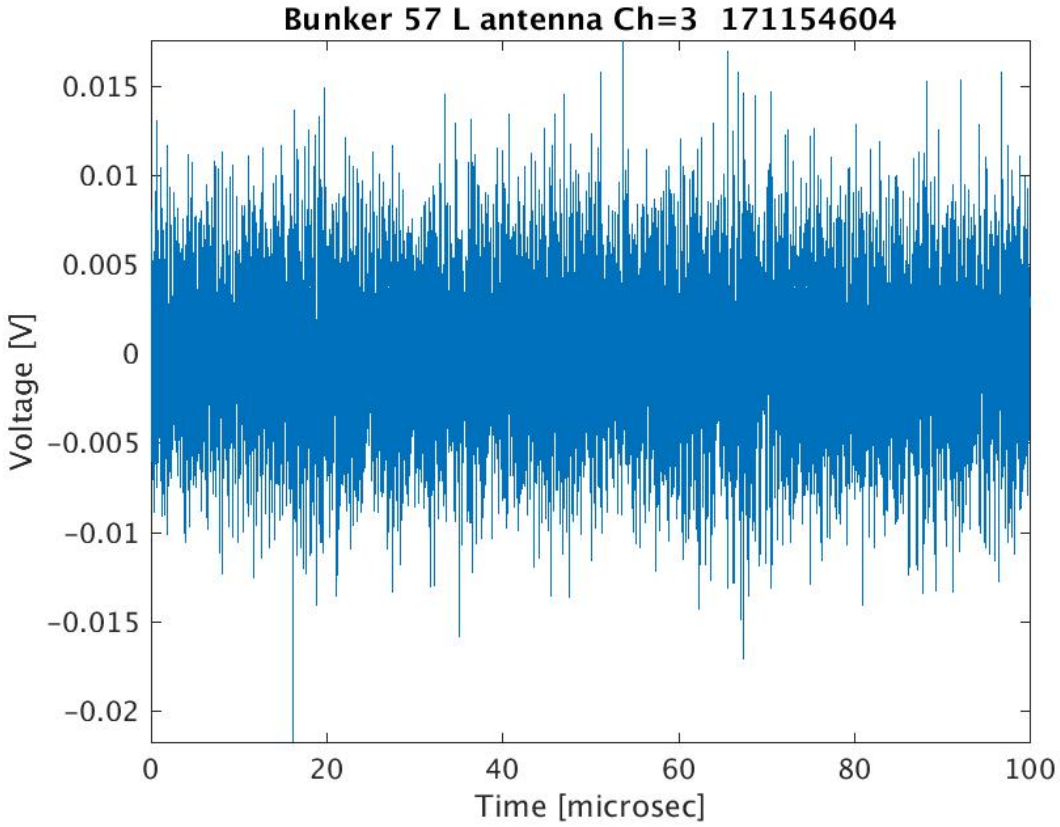

Figure 5.4: Collect from Channel 3 of the Bunker 57 data acquisition system. The signal at $\approx 18\,\mu$s after the top of the GPS minute is due to the capacitor bank discharge. The weak signal at $\approx 64\,\mu$s is from the firing of the EFF system. These events are seen better in Figure 5.5. The figure labeling uses the data acquisition system's internal clock. This is several seconds behind the actual GPS time.

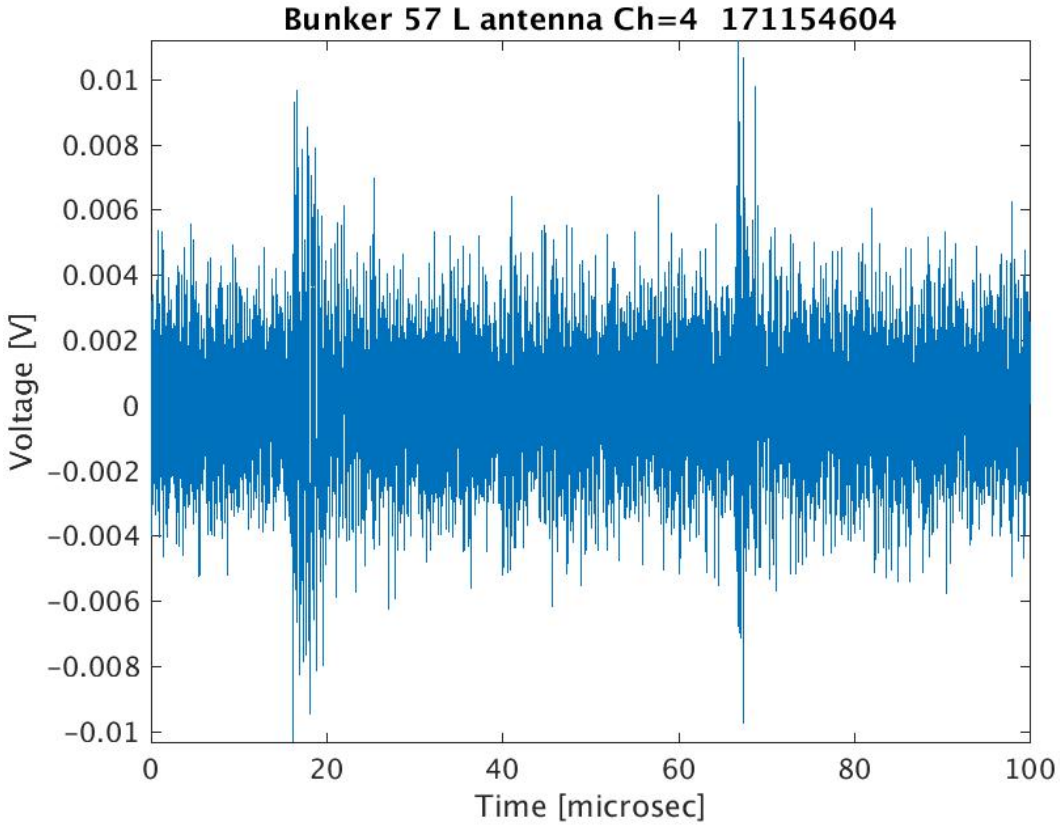

Figure 5.5: Collect from Channel 4 of the Bunker 57 data acquisition system. The signal at $\approx 18\,\mu$s after the top of the GPS minute is due to the capacitor bank discharge. The weak signal at $\approx 64\,\mu$s is from the firing of the EFF system. The figure labeling uses the data acquisition system's internal clock. This is several seconds behind the actual GPS time.

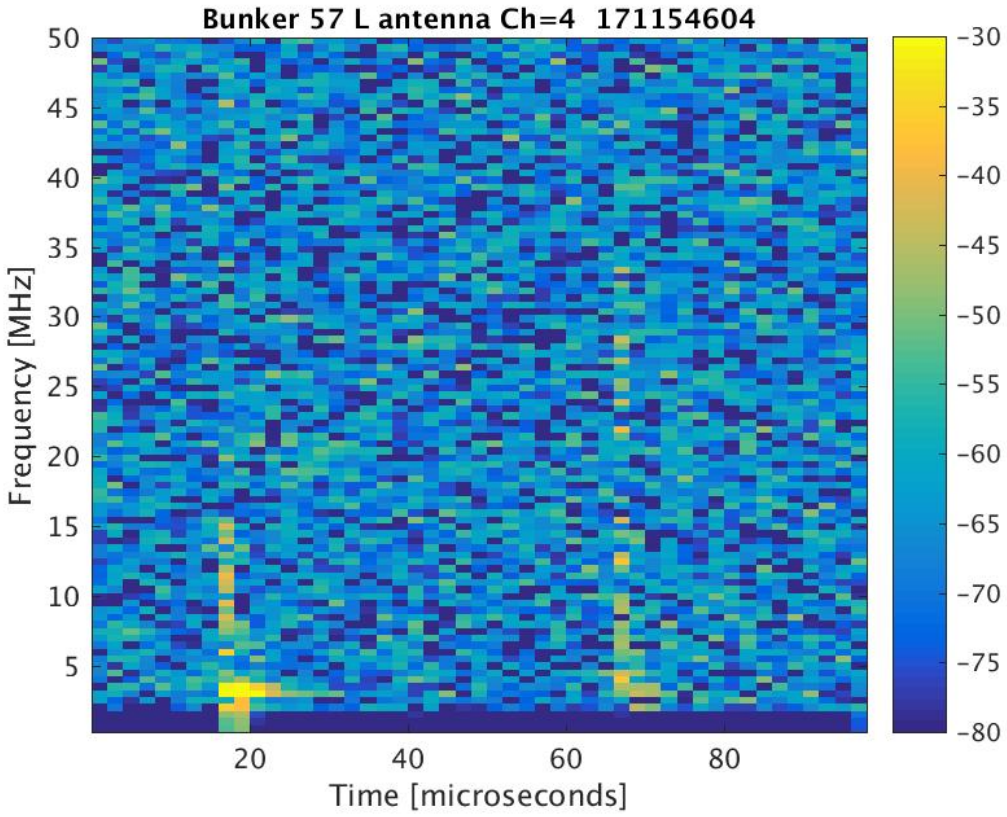

Figure 5.6: Spectrogram of Channel 4 of the Bunker 57 data acquisition system. The signal at ≈18 μs after the top of the GPS minute (0 microseconds) is due to the capacitor bank discharge. The weak signal at ≈64 μs is from the firing of the EFF system. The capacitor bank has most of its radiated energy below 15 MHz while the EFF shot has signals up to 35 MHz. The data have been high-pass-filtered to remove interference and noise below 1.5 MHz. The figure labeling uses the data acquisition system's internal clock. This is several seconds behind the actual GPS time.

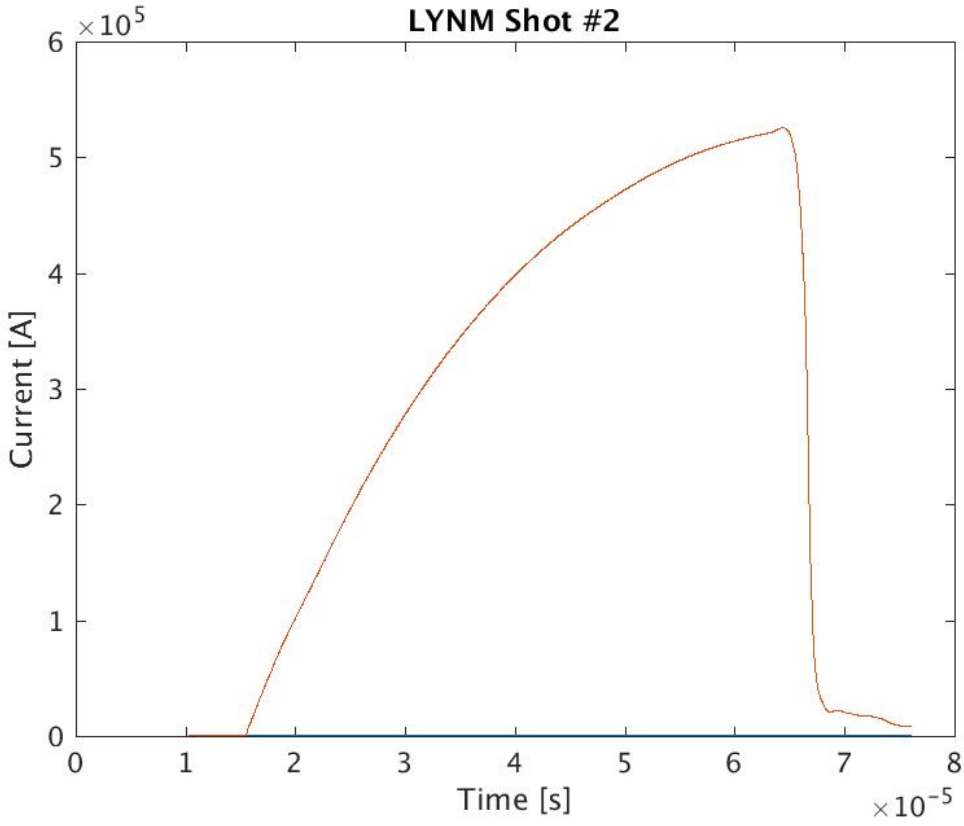

Figure 5.7: Loop current as function of time for the second EFF test. The timestamps have been offset by 10 μs to make the timing consistent with the other data used in this report.

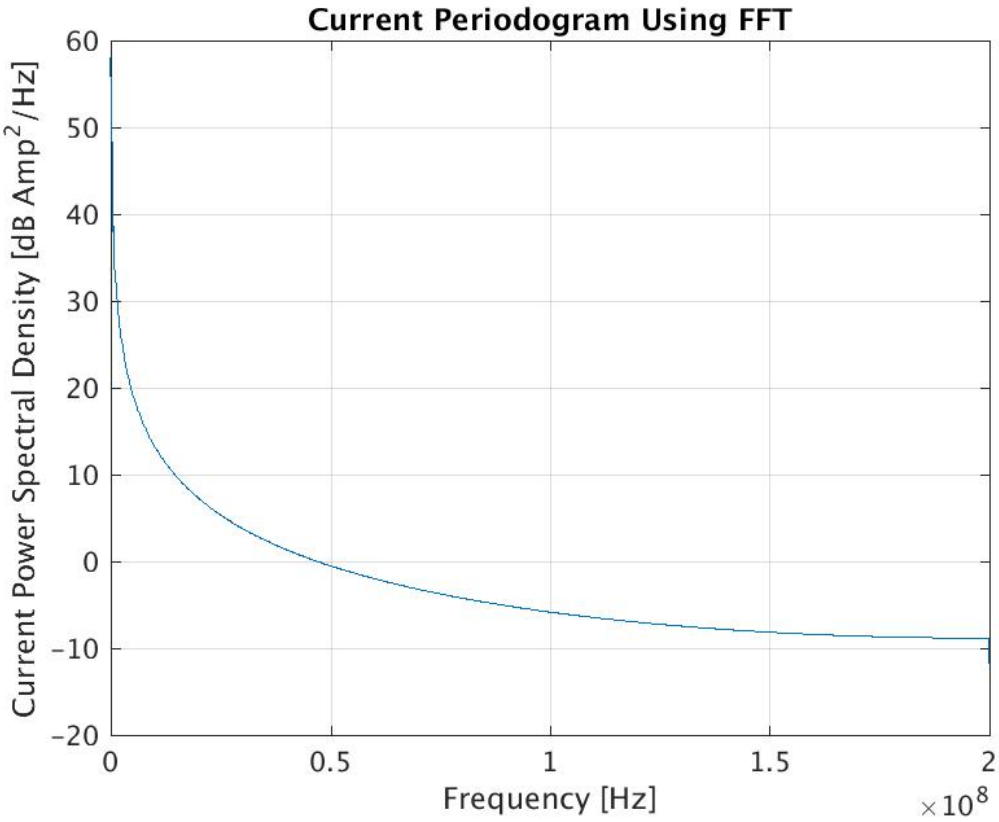

Figure 5.8: EFF loop current power spectral density for the second EFF test. The spectral bin width is 1.667×10^5 Hz.

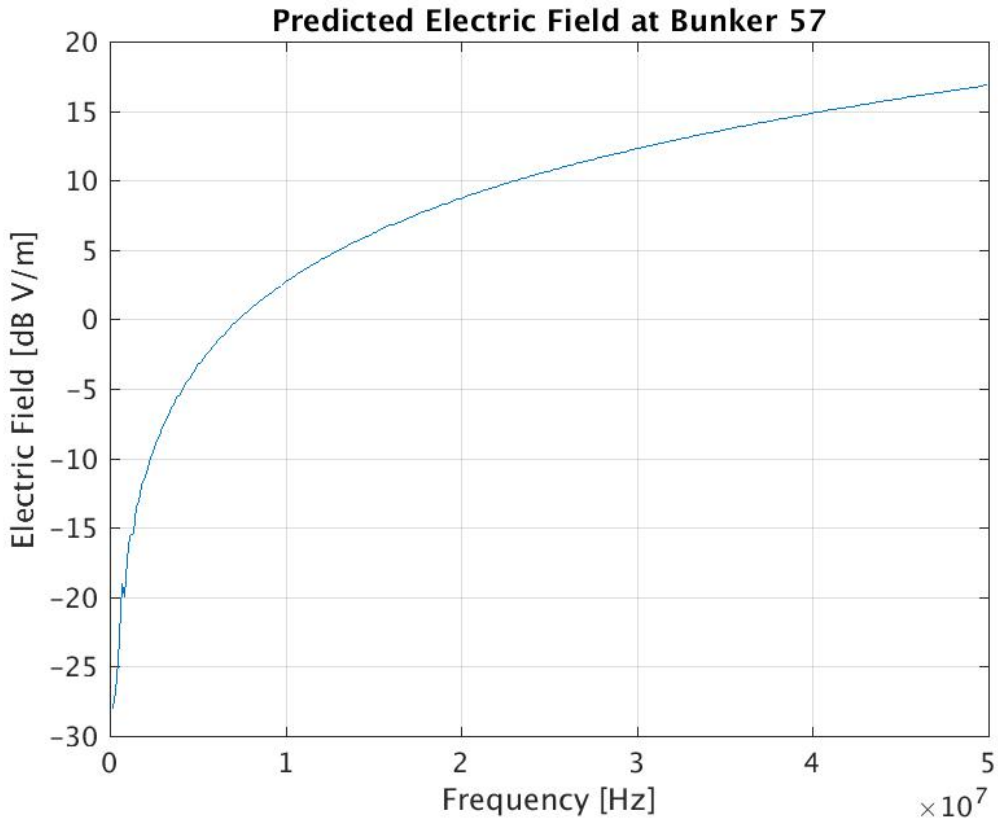

Figure 5.9: Predicted electric field strength at Bunker 57 L antenna for the second EFF test.

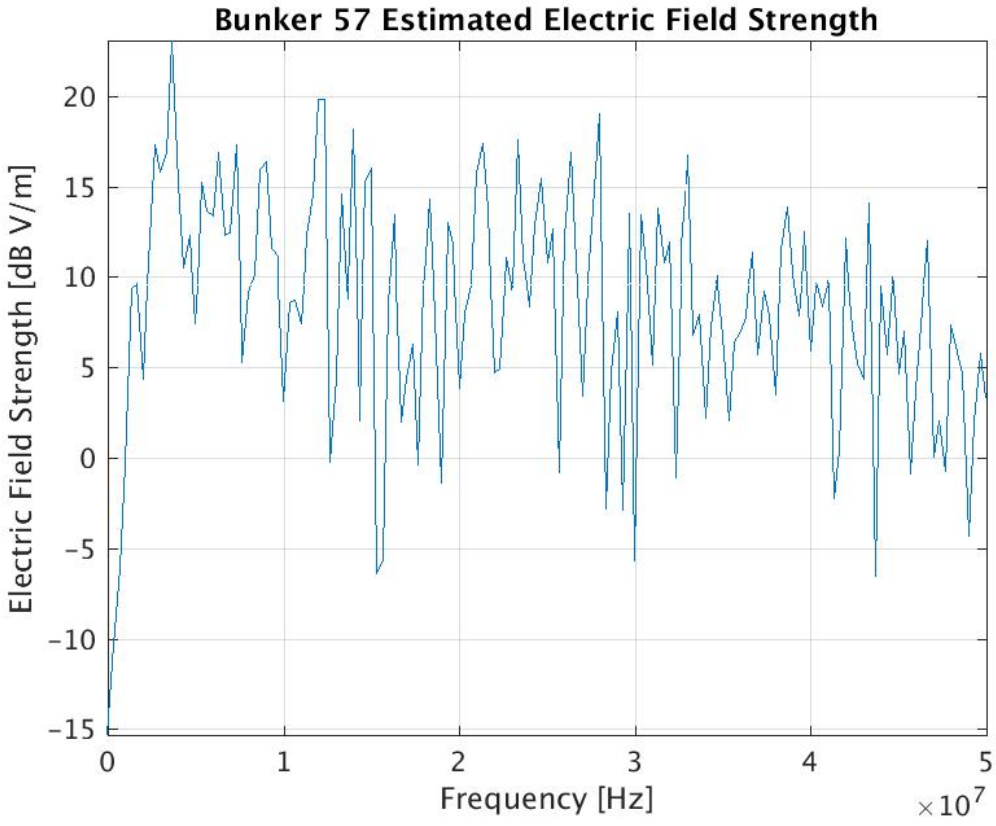

Figure 5.10: Estimated electric field strength at Bunker 57 L antenna for the second EFF test using the data from the L antenna, channel 4. The calculation adopts 3 dB splitter loss, 3.2 dB cable loss, and an Antenna Factor of 23 dB(1/m).

5.3 At Point 88 firing point

5.3.1 Dry run

Below, we show the signals collected on the 2 Centerfire discones ("Discone 1", "Discone 2") at the Point 88 firing point (Figures 5.11, 5.12, 5.13, 5.14). There are 4 channels (channels 1 – 4) for each discone because we bracketed the voltage ranges on the data acquisition systems. The signals source was the firing of a bridgewire.

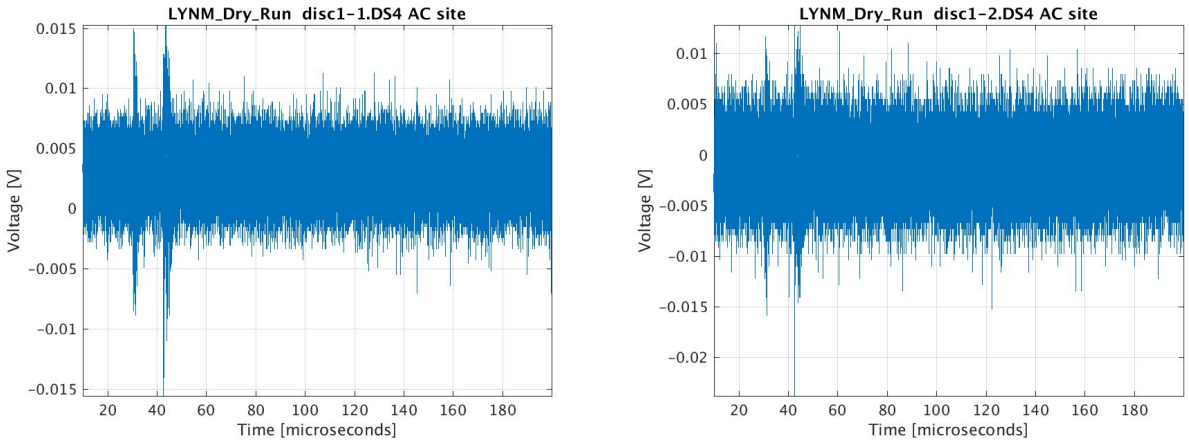

Figure 5.11: Bridgewire test shot at the Point 88 Firing Point: Discone 1, Channel 1 (left) and Channel 2 (right). The data have been shifted by the known amount of 10 μs to maintain consistency with the other RF collection systems.

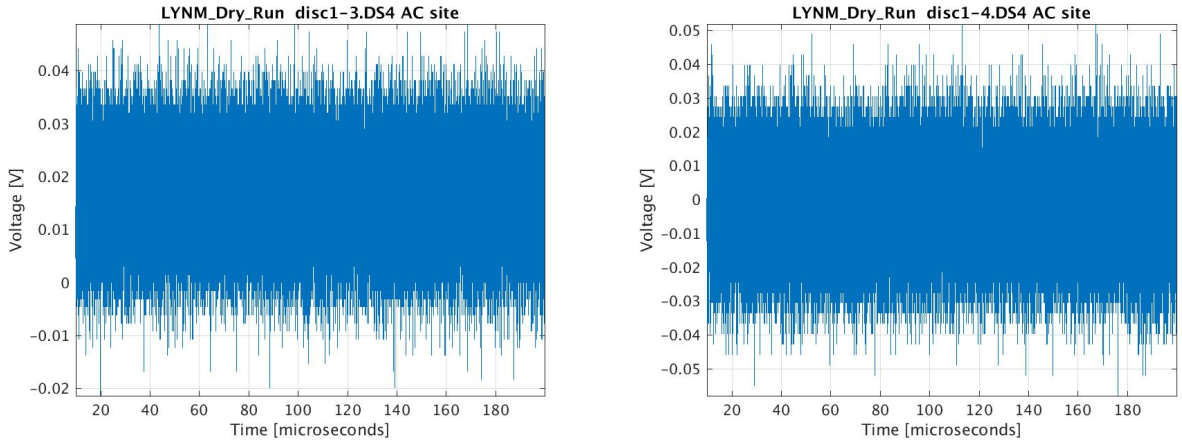

Figure 5.12: Bridgewire test shot at the Point 88 Firing Point: Discone 1, Channel 3 (left) and Channel 4 (right). The data have been shifted by the known amount of 10 μs to maintain consistency with the other RF collection systems.

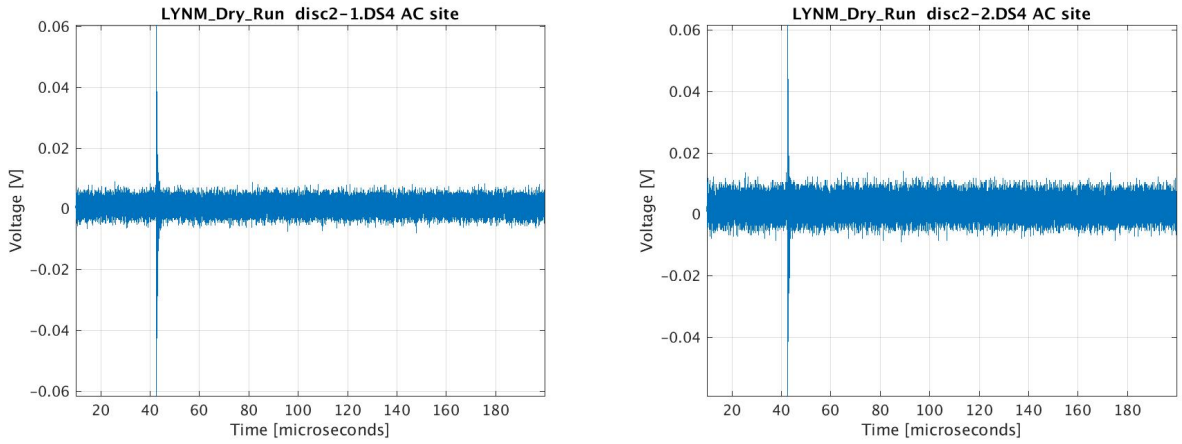

Figure 5.13: Bridgewire test shot at the Point 88 Firing Point: Discone 2, Channel 1 (left) and Channel 2 (right). The data have been shifted by the known amount of 10 μs to maintain consistency with the other RF collection systems.

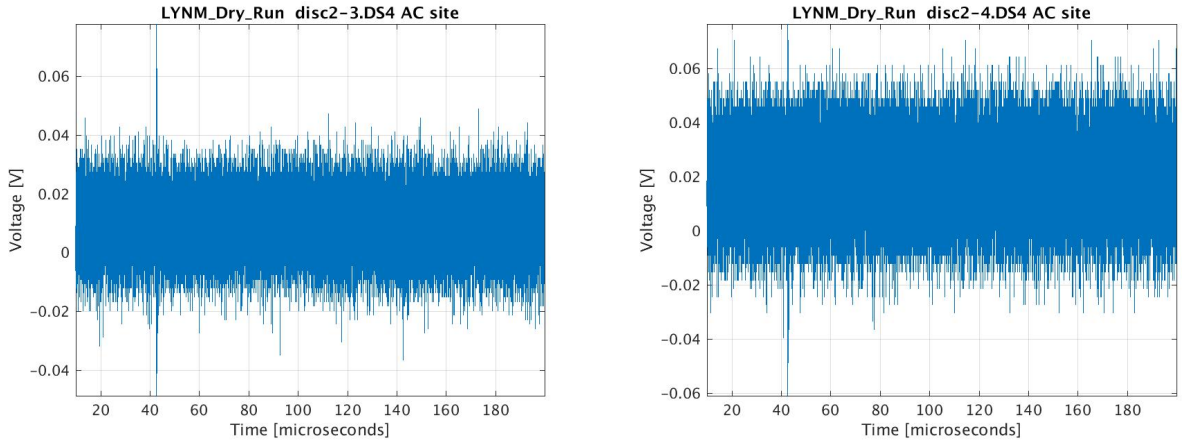

Figure 5.14: Bridgewire test shot at the Point 88 Firing Point: Discone 2, Channel 3 (left) and Channel 4 (right). The data have been shifted by the known amount of 10 μs to maintain consistency with the other RF collection systems.

5.3.2 EFF shot

Figures 5.15, 5.16, 5.17 and 5.18 show the RF signals collected on the 2 discones at the Point 88 firing point. The data ranges on the digital oscilloscopes were bracketed to avoid saturation on all channels. However, all channels are still saturated. The least saturated channels are Channel 4 on each of the discones.

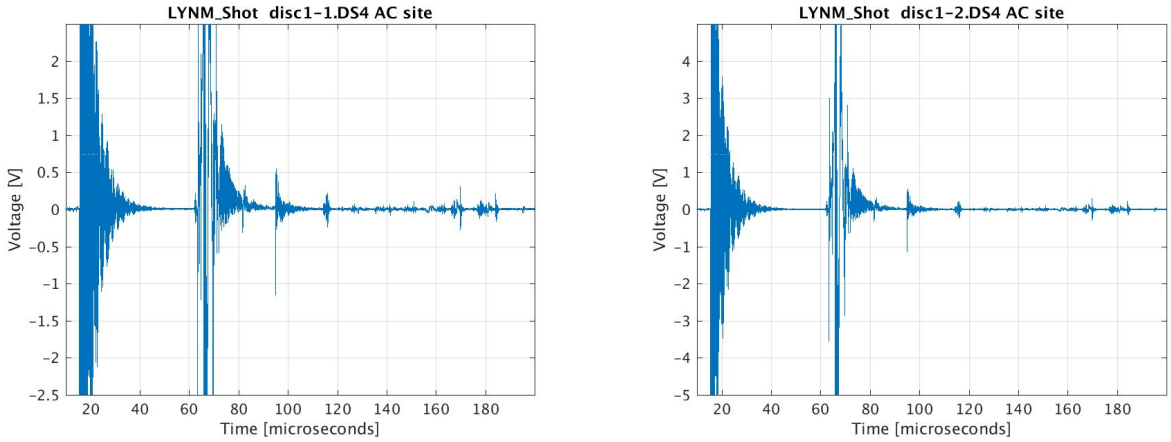

Figure 5.15: EFF shot at the Point 88 Firing Point: Discone 1, Channel 1 (left) and Channel 2 (right). The data have been shifted by the known amount of 10 μs to maintain consistency with the other RF collection systems.

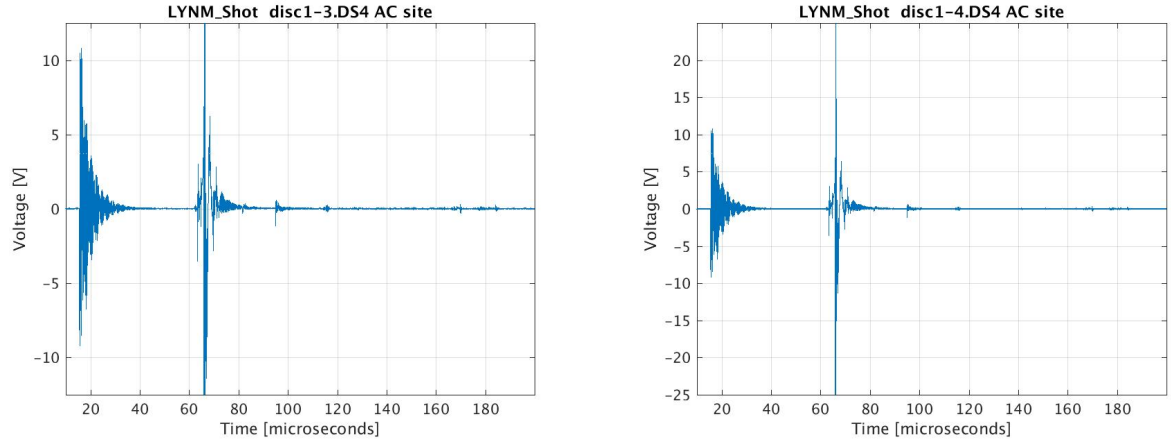

Figure 5.16: EFF shot at the Point 88 Firing Point: Discone 1, Channel 3 (left) and Channel 4 (right). The data have been shifted by the known amount of 10 μs to maintain consistency with the other RF collection systems.

We also see standing waves in the signals collected by the near-field antennas *e.g.* Figure 5.19. The nulls occur every 19 MHz *i.e.* at multiples of $\lambda/2 = 15.8\,\mathrm{m}$. This corresponds to a length of $27.7\,\mathrm{m} \times (\text{velocity factor})^{-1}$. The standing wave pattern may be in the RF collection cables or it may be in the cables used to excite the EFF loop itself. Since we see slightly different standing wave patterns for the 2 discones, we believe the standing wave patterns to be associated with the cabling from the antennas to the data acquisition systems in the bunker.

At 3.67 MHz, we see $2.032 \times 10^{-7}\,\mathrm{V^2\,Hz^{-1}}$ in a 100 kHz frequency bin. Scaling for an assumed value of the Antenna Factor of $23\,\mathrm{dBm^{-1}}$, a 4-way splitter loss of 3dB per channel and 2 dB of loss in the cables from the antenna to the data acquisition system, we estimate that the electric field strength at this frequency is $11\,\mathrm{dBV\,m^{-1}}$. The peak voltage power spectral density is seen at about 400 kHz ($1.705 \times 10^{-5}\,\mathrm{V^2\,Hz^{-1}}$) and the resulting estimated electric field is $32.8\,\mathrm{V\,m^{-1}}$.

5.4 On East Mesa

We failed to collect any signals during the EFF shot event. The data collection system was enabled and collecting signals correctly at the top of each minute from about 1:45 p.m. onwards on shot day. The system UPS system ran out of power at about 5:02 p.m. The actual EFF shot occurred at 5:12 p.m.

The UPS system was scaled for a nominal 4 hour lifetime at 800 W consumption. The UPS system had been fully charged when we started the data collect.

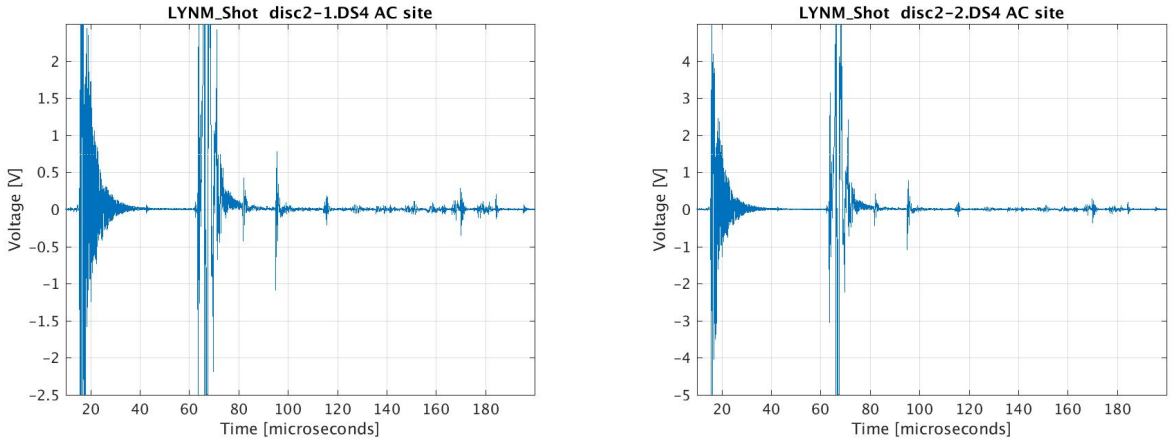

Figure 5.17: EFF shot at the Point 88 Firing Point: Discone 2, Channel 1 (left) and Channel 2 (right). The data have been shifted by the known amount of 10 μs to maintain consistency with the other RF collection systems.

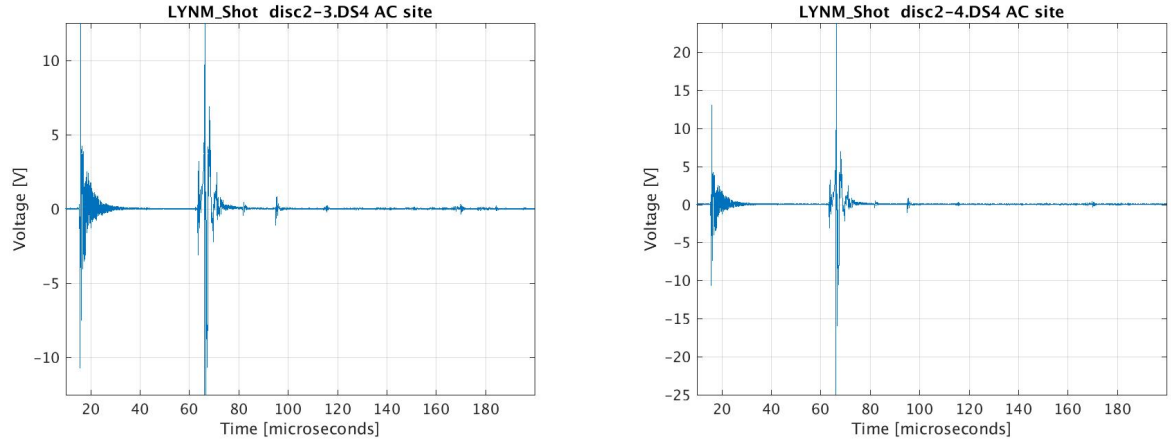

Figure 5.18: EFF shot at the Point 88 Firing Point: Discone 2, Channel 3 (left) and Channel 4 (right). The data have been shifted by the known amount of 10 μs to maintain consistency with the other RF collection systems.

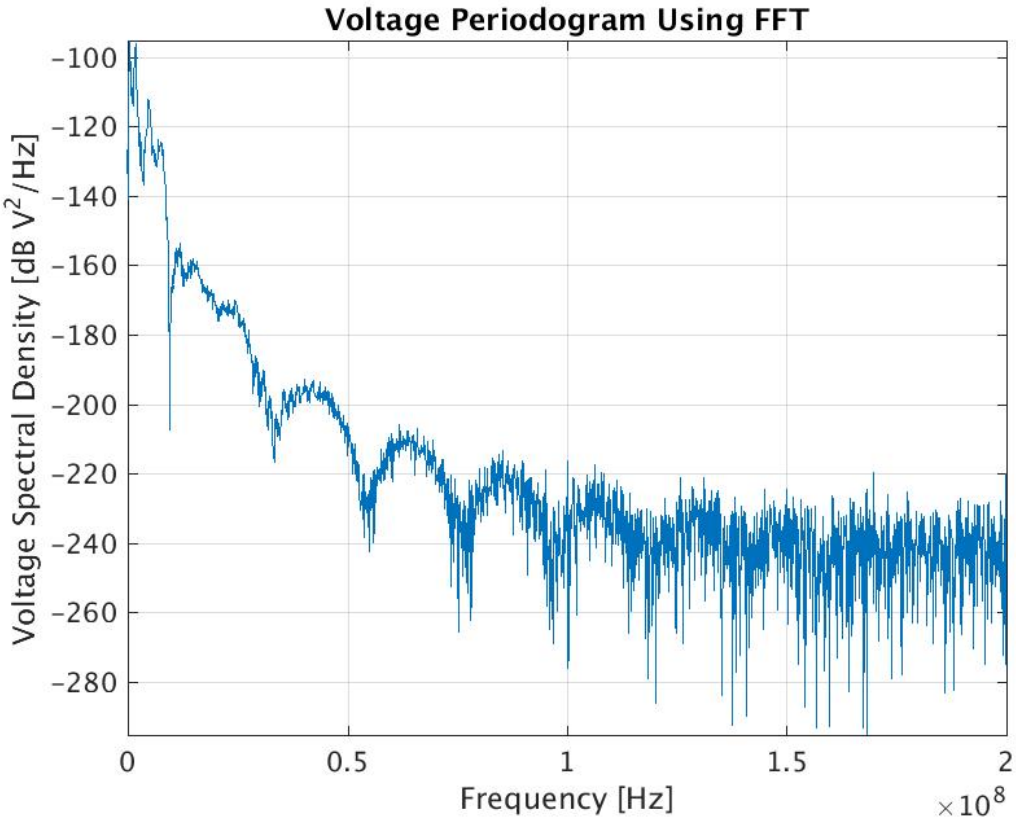

Figure 5.19: Voltage Power Spectral Density for discone 2, channel 4, at the Point 88 location during EFF shot.

5.5 Discussion

The voltage power spectral density at the peak frequency (3.7 MHz) at the Bunker 57 collection point was $0.596\,\mathrm{V\,m^{-1}}$. Scaled for the distance to the East Mesa collection point and compensating for the different orientations with respect to the loop axis, we predict an electric field strength at this frequency of $0.351\,\mathrm{V\,m^{-1}}$ on the East Mesa.

Using the nominal Antenna Factor for the Rohde & Schwarz HE010 antennas ($17\,\mathrm{dB\,m^{-1}}$), we predict a voltage at the output of the antenna of -26.1 dB V or 49.6 mV.

From the March 2017 collects, the noise floor in this 100kHz channel was 0.113 mV (Figure 5.20). Thus we predict that we would have had a substantial signal-to-noise ratio at the East Mesa (53 dB) had the collection system been running.

If we scale the predicted signal on the East Mesa for the June 2017 experiment for the smaller loop size in the March experiment (March: 2.6 cm × 35.5 cm; June: 44 cm × 44 cm), and compensate for the different orientations of the collection location with respect to the loop axis, then we predict that we would have had an SNR of 3.99 (in voltage) *i.e.* 12.0 dB in a 100 kHz spectral bin for the March experiment. (We used the same location and the same antennas for both collects on the East Mesa.)

Armed with our knowledge of the EFF EM spectrum, we have revisited our analysis of the March 2, 2017, data. We have bandpass-filtered (2–5MHz) the HE010 antenna data on the East Mesa at the time of the shot, aligned these in time through cross-correlation, and summed the data from all antennas. The smoothed result is plotted in Figure 5.21. We see a voltage pulse with a peak of 5.5 mV at ≈55.5 μs which is roughly at the correct time. However, we also see an earlier pulse of about the same strength at ≈43 μs. The difference in times does not correspond to that for the two significant events in the firing of the EFF shot *viz.* the discharge of the capacitor bank and the firing of the EFF. The EM radiation from the discharge of the capacitor bank is not quite as strong as that from the firing of the EFF. (See Figure 5.6.) The peak signal at 55.5 μs is about what we would have expected for the March 2, 2017, EFF configuration.

Thus, we conclude that we *may* have detected the firing of the EFF in the March 2017 experiment but we cannot be sure.

5.6 Recommendations

- Because the new EFF loop configuration appears to have worked well, we should use something very similar for the next test shot in Ancho Canyon.
- In the scenarios for the larger scale experiments (not at Ancho Canyon), we will need to re-visit how we implement an effective RF radiator.
- The RF collection needs to be an **integrated** part of the whole experiment in future tests. This means that the RF collection and the EFF shot components need to be considered together in a comprehensive experiment plan.
- For larger scale shots, including the large Ancho Canyon test in FY18, there will need to be more formality of operations.

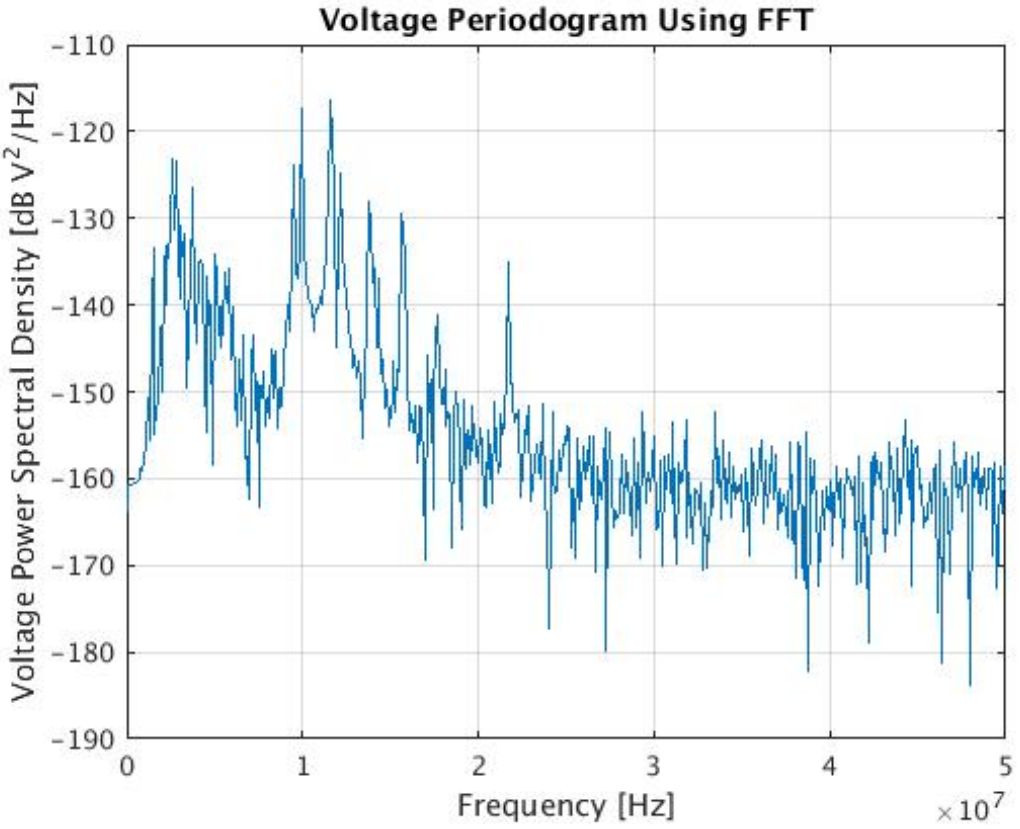

Figure 5.20: Noise floor on the East Mesa from the March 2017 collects. The spectral bin width is 100 kHz.

- The larger scale tests will also have a seismo-acoustic component and this will also need to be incorporated into the comprehensive experiment plans.
- The RF collection always needs to include some redundancy in the form of extra collection stations.
- The RF collection team needs to evaluate collection system running time under the expected load for the UPS systems.
- The RF collection systems may need either extra UPS capacity and/or automatic or controlled switch-over from generator power to UPS power.

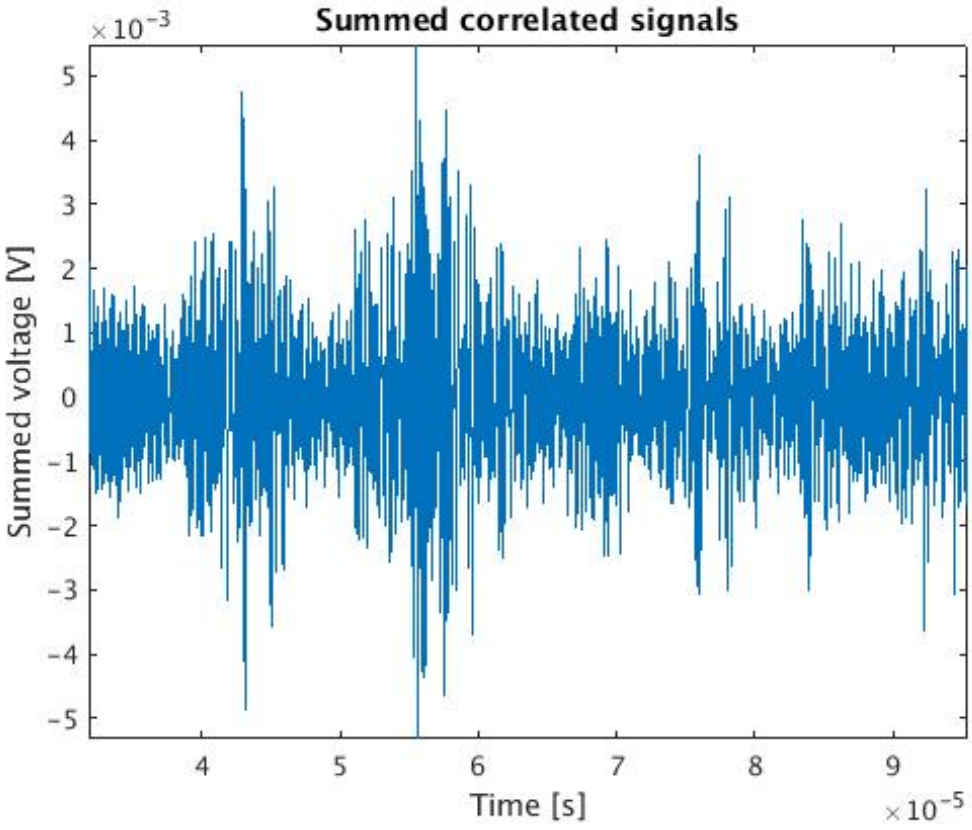

Figure 5.21: Bandpass filtered, temporally-aligned, summed voltage data from collects on HE010 antennas on East Mesa at time of March 2, 2017, EFF shot. The pulse at 55.5 μs *may* be the signature of the EFF but this identification is not robust.

Chapter 6

Revision history

6.1 Revisions

- June 15, 2017: v.1.0: Initial version.
- July 7, 2017: v.1.1: Fixed LaTeX errors. Added electric field analysis. Added Firing Point figures after extensive renaming.
- July 10, 2017: v.1.2: Fixed a plot scaling error for PSD plots. Numerical calculations were correct but plots were improperly scaled. Labeled plots correctly now — channels 3 and 4 were on L antenna at Bunker 57.
- July 10, 2017: v.1.3: Added pictures of setups. Inserted Ho, Frigo & Haynes (2014) reference.
- July 11, 2017: v.1.4: Added Google Earth maps with annotations.
- July 12, 2017: v.1.5: Added re-visited analysis of March 2, 2017, East Mesa data at time of shot.
- August 10, 2017: v.1.6: Many typos fixed.
- August 14, 2017: v.1.7: Added plot to show estimated electric field strength at Bunker 57 using measured data. The corresponding plot of the predicted field strength was rescaled to match.
- August 15, 2017: v.1.8: Replaced timing diagram (Figure 5.1) with better version. Generated FINAL version.
- September 11, 2017: v.1.9: Removed "Official Use Only" label from footer since this document is unclassified and uncontrolled.
- September 18, 2017: v.1.10: Minor typos fixed.

Bibliography

Aaronia 20100e, 2014,
`http://www.aaronia.com/products/antennas/BicoLOG-20100E-EMC-Antenna/`,
accessed July 8, 2014

AIR, 2017,
`https://www.air802.com/Ultra-Wideband-Shortwave-Discone-Antenna-100-to-1000-MHz-1-to-3.5-dBi-Gain.html`,
accessed June 26, 2017

Antenna Research Associates 2017,
`www.ic72.com/pdf_file/d/103797.pdf`,
accessed June 26, 2017

Aaaronia 2017,
`http://www.aaronia.com/products/antennas/BicoLOG-20100E-EMC-Antenna/`,
accessed June 26, 2017.

Balanis, C. A. 2005,
"Antenna Theory: Analysis and Design",
John Wiley & Sons, Hoboken, NJ, p.242

Burke, G.J. and Poggio, A.J. 1981,
"Numerical Electromagnetics Code (NEC) – Method of Moments / Part I: Program Description – Theory",
Lawrence Livermore National Laboratory, UCID-18834

Burke, G.J. and Poggio, A.J. 1981,
"Numerical Electromagnetics Code (NEC) – Method of Moments / Part II: Program Description – Code",
Lawrence Livermore National Laboratory, UCID-18834

Burke, G.J. and Poggio, A.J. 1981,
"Numerical Electromagnetics Code (NEC) – Method of Moments / Part III: User's Guide",
Lawrence Livermore National Laboratory, UCID-18834

Burke, G.J. 1992,
"Numerical Electromagnetics Code — NEC-4 – Method of Moments / Part 1: User's

Manual (NEC-4.1)",
Lawrence Livermore National Laboratory, UCRL-MA-109338 Pt.1

Centerfire Antennas, 2017,
http://centerfireantenna.com/antenna-menu/deluxe-discone-antenna/
accessed January 26, 2017

Diamond Antenna, 2017,
http://www.diamondantenna.net/d130nj.html,
accessed June 22, 2017

Goforth, J. 2017,
"EFF 107 Pulsed Power Results",
LANL internal project report, March 9, 2017

Hascall-Danke, 2017,
http:\www.hascall-denke.com/wp-content/.../113-420-MHz-1Y00019-FXDC113X4.pdf,
accessed June 21, 2017

Ho, C., Frigo, J.R. and Haynes, W.B. 2014,
"Fieldable Impulsive Source and Timer (FIST)",
Los Alamos National Laboratory, LA-UR-14-29053, November 21, 2014

Junor, W., Layne, J., Gamble, T., Quintana, B., Snelson-Gerlicher, C. and Goorley, T. 2017,
"Ancho Canyon RF Collect, March 2, 2017: Final Report",
LANL, August 14, 2017.

Kraus, J.D. and Marhefka, R.J. 2002,
"Antennas for all applications", McGraw-Hill, p.197

MiniCircuits (2017),
https://www.minicircuits.com/pdfs/BLP-50+.pdf,
accessed March 29, 2017

OSHA: Occupational Safety and Health Administration, United States Department of Labor, 1990,
https://www.osha.gov/SLTC/radiofrequencyradiation/electromagnetic_fieldmemo/elecEtromagnetic.html,
accessed April 4, 2017

Rohde & Schwarz HE010 2017,
https://www.rohde-schwarz.com/us/product/he010-productstartpage_63493-9361.html,
accessed April 6, 2017

Rohde & Schwarz IN115 2017,
`https://www.rohde-schwarz.com/us/product/in115-productstartpage_63493-9363.html`,
accessed March 29, 2017

Rosa, E.B. and Grover, F.W. 1912,
"Formulas and tables for the calculation of mutual and self-inductance (revised)",
Volume 8, National Bureau of Standards, pp.154–155

Topcon 2017,
`https://www.topconpositioning.com/`,
accessed March 29, 2017